Journal of Physics and Chemistry of Solids 175 (2023) 111198

Contents lists available at ScienceDirect

Journal of Physics and Chemistry of Solids

journal homepage: www.elsevier.com/locate/jpcs

Pressure effect on the structural, electronic, and magnetic properties of the battery cathode material $LiMn_2O_4$: An *ab-initio* study

O.M. Sousa [a,*], F. Sorgenfrei [b], L.V.C. Assali [a], M.V. Lalic [c], A.B. Klautau [d], P. Thunström [b], C.M. Araujo [b,e,**], O. Eriksson [b], H.M. Petrilli [a]

[a] Universidade de São Paulo, Instituto de Física, Rua do Matão, 1371, 05508-090, São Paulo, SP, Brazil
[b] Uppsala University, Department of Physics and Astronomy, Box 516, SE-75120, Uppsala, Sweden
[c] Universidade Federal de Sergipe, Departamento de Física, 49100-000, São Cristóvão, SE, Brazil
[d] Universidade Federal do Pará, Faculdade de Física, 66075110, Belém, PA, Brazil
[e] Karlstad University, Department of Engineering and Physics, 65188, Karlstad, Sweden

ARTICLE INFO

Keywords:
Cathode materials
$LiMn_2O_4$ under pressure
Electronic structure

ABSTRACT

$LiMn_2O_4$ is a battery cathode material with desirable properties such as low cost, low toxicity, high natural abundance of Mn, and environmental compatibility. By means of first-principles calculations, we study the structural, magnetic, and electronic properties of $LiMn_2O_4$ under ambient conditions and high hydrostatic pressures (until 20 GPa). We obtain two oxidation states for Mn, even using a cubic structure, which differ in all analyzed properties: structural, electronic, and magnetic. At $P > 0$, such properties were found to display a standard behavior decreasing smoothly and linearly with pressure. Furthermore, the enthalpy of cubic and orthorhombic structures under low and high-pressure conditions were examined, showing that no cubic to orthorhombic phase transition exists in all the investigated pressure range, nor is a magnetic cubic to a non-magnetic cubic phase transition possible.

1. Introduction

Electric batteries are electrochemical stores of clean and renewable energy and, therefore, are devices considered able to replace fossil fuels. Lithium-ion batteries (LIBs) have become the main battery stream for portable devices due to their high energy storage capacity, life cycle, environmental compatibility, and more effortless mobility than lead-acid batteries. This type of battery is used in cell phones, laptops, tablets, and electric vehicles [1,2].

During the choice of material to produce LIBs, some factors must be considered, for example, how the cathodic and anodic materials behave under the effects of temperature or pressure. These effects can strongly influence the electrochemical performance of cathode materials in the battery environment. Therefore, investigating the effects of pressure and temperature on cathodic and anodic materials is extremely important. Understanding the behavior of the structural properties of lithiated transition metal oxides under high pressure can provide valuable information about the control of the mechanical and electrochemical processes that occur during the charge/discharge process of lithium batteries [3]. In this work, we analyze the effects of hydrostatic pressure on lithium manganese oxide ($LiMn_2O_4$, LMO).

LMO is a cathode material with desirable properties belonging to a class of materials that enable the formation of greener and more sustainable batteries for electrical energy storage [4–7]. This compound has a high Li intercalation potential showing good energy density in batteries that use it as cathodic material. At ambient conditions, the LMO crystallizes in a partially inverse spinel structure with space group $Fd\bar{3}m$. Manganese ions are located at 16d octahedral sites, half of them exhibiting 3+, and other half 4+ oxidation state. Li ions preferentially occupy 8a tetrahedral sites, but in the discharge process, they can occupy 16c empty octahedral sites. Oxygen ions occupy position 32e. The Li-ion can be removed and reversibly inserted into the structure at a very high voltage (4 V), with a theoretical specific capacity of 148 mAh/g. The structure of the LMO forms a rigid three-dimensional network that favors the transport of Li ions. The channels for Li insertion and disinsertion are formed by connecting the 8a tetrahedral sites with the empty 16c octahedral sites. Li ions are mobile within these

* Corresponding author.
** Corresponding author. His Uppsala University, Department of Physics and Astronomy, Box 516, SE-75120, Uppsala, Sweden.
E-mail addresses: osmarufpa@gmail.com (O.M. Sousa), moyses.araujo@physics.uu.se (C.M. Araujo).

https://doi.org/10.1016/j.jpcs.2022.111198
Received 25 November 2022; Received in revised form 21 December 2022; Accepted 22 December 2022
Available online 30 December 2022

channels along the 8a-16c-8a path. In this compound, Mn^{3+} (configuration: e^2_g, b^1_{2g}, a^1_{1g}, b^0_{1g}) is a Jahn-Teller (JT) active ion. On the other hand, Mn^{4+} (configuration: t^3_{2g}, e^0_g) is not a JT active ion [8–10].

In recent years, density functional theory (DFT) [11,12] has been widely used to study energy storage [13]. Through this theory, several important contributions have been made to the understanding of electrochemical reactions. This theory is also very useful for investigating the effects of pressure on materials. In this work, we use DFT to investigate different physical and chemical properties of LMO under ambient conditions and at high hydrostatic pressures ($0 \leq P < 20$ GPa).

LMO under hydrostatic and non-hydrostatic pressure has already been investigated experimentally. The pioneering work of LMO under non-hydrostatic pressure ($0 \leq P < 2.6$ GPa) revealed, by X-ray diffraction, a transition from cubic to tetragonal phase [14]. Most other works that investigated this compound under hydrostatic and non-hydrostatic pressure also proposed a cubic → tetragonal phase transition [3,15–17]. Lin et al. [3] showed that when non-hydrostatic pressure of around 0.4 GPa is applied, the LMO already undergoes an irreversible cubic → tetragonal phase transition. These authors also showed that the structure of LMO under hydrostatic pressure remains cubic even at 10 GPa. In turn, Paolone et al. [18] investigated the LMO under hydrostatic pressure, also by X-ray diffraction, and found a cubic → orthorhombic transition at 1.8 ± 0.4 GPa. Most previous works cite the results obtained by Paolone et al. but do not describe any additional information about the possible cubic → orthorhombic transition. Lin et al. [3] described the work of Paolone et al. as a suggestion of an orthorhombic phase without additional structural information. Piszora [17], in a brief commentary, described that the nature of this transition (cubic → orthorhombic) seems to be not so clear. The cubic → orthorhombic phase transition has been concluded from profile broadening of the cubic (311) and (400) reflections compared to (111) and (222) lines. Piszora [17] describes that due to the low resolution it was not possible to observe the division of these lines. In conclusion, according to the experimental works published so far, a consensus about the existence of the cubic → orthorhombic phase transitions under hydrostatic pressure has not been reached. A theoretical investigation of the LMO under pressure is therefore fundamental for understanding this eventual transition. By calculating the enthalpy, it is possible to confirm the existence or absence of the orthorhombic phase which can help the experimental work. Therefore, the main goal of this work is to investigate the possible cubic → orthorhombic phase transition of the LMO from first principles theory. To verify this structural transition, it is necessary to correctly simulate the material in the cubic phase, a task that faces some difficulties. Namely, the standard simulation of the cubic $Fd\bar{3}m$ space group (n ° 227) does not allow for a JT distortion around the Mn^{3+} ions, once all the Mn are equivalent, i.e., the spontaneous symmetry breaking is not trivially possible. The LMO cubic phase is stable under ambient conditions. However, below 280 K there is a cubic → orthorhombic phase transition [14]. Therefore, the orthorhombic structure must be the ground state structure, as shown by our results at $P = 0$ for this material (see below).

Due to the difficulty of simulating the cubic structure of the LMO, and due to the fact that the orthorhombic structure is the ground state, most of the previous calculations always resorted to the orthorhombic phase to observe different oxidation states of Mn, allowing them to observe the JT distortion of the oxygen atoms surrounding the Mn^{3+} ion, and correctly describing the semiconducting state of LMO [8,19–21]. These properties could not be observed for a cubic phase restricted to the $Fd\bar{3}m$ space group, where the Mn atoms are all equivalent. On the other hand, the calculations of the cubic phase are fundamental in describing the possible transition between the cubic and the orthorhombic phase. Accordingly, the simulation of the cubic phase was the primary objective of this work. The details of this simulation are described in section 2. By applying some simple computational tricks, we were able to observe different oxidation states for Mn in all properties analyzed for the cubic structure: structural (different bond lengths for Mn^{3+} and Mn^{4+} ions), electronic (different density of states for Mn^{3+} and Mn^{4+} ions), and magnetic (different magnetic moments for Mn^{3+} and Mn^{4+} ions). Previously, a successful simulation of the cubic phase of the LMO has been reported only in Ref. [22], but the authors did not notify which magnetic ordering has been considered in their calculations, information that is essential for the determination of the enthalpy.

Finally, on the base of the calculated enthalpies of the LMO in cubic and orthorhombic phases, we concluded that the cubic phase persists in the whole range of investigated pressures (0–12 GPa), discarding the occurrence of the cubic → orthorhombic phase transition. Additionally, we also discarded the existence of the cubic magnetic → cubic non-magnetic phase transition in the same pressure range.

2. Method and calculations details

In this work, the $LiMn_2O_4$ was simulated using the all-electron spin-polarized full-potential linearized augmented plane wave (FP-LAPW) method [23], implemented in the WIEN2k computational package [24], within the framework of the density functional theory [11,12]. In this method, the electronic wave functions are expanded into spherical harmonics within the atomic spheres and into plane waves in the interstitial region. In the atomic regions, a spherical harmonic basis set was used with azimuthal quantum number up to $\ell_{max} = 10$. Convergence in the total energy was achieved using a $K_{max} = 7.0/R_{MT}$ parameter, which defines the total number of plane waves describing the electronic wave functions in the interstitial region, where R_{MT} is the smallest radii of the atomic spheres, which were chosen to be $R_{MT}(Mn) = 1.70$, $R_{MT}(O) = 1.6$, and $R_{MT}(Li) = 1.5$ atomic units (a.u.). The valence electrons configurations were Li: $2s^1$, Mn: $3s^2 3p^6 3d^5 4s^2$, and O: $2s^2 2p^4$. Self-consistent iterations were performed until the total energy converged within the accuracy of 10^{-5} Ryd. 32 k-point mesh was used for the integration in the irreducible part of the Brillouin zone. The exchange-correlation effects were treated by the generalized gradient approximation [25] plus the on-site Hubbard U [26–28] potential to describe in a mean field approximation the electronic correlation among the Mn-3d electrons. The $U = 4.2$ eV has been applied, which is among the values that already have been used to describe several properties of the LMO [29,30]. Formation energy, average voltage, and theoretical specific capacity were calculated according to equations S1, S2, and S3 of the supplementary information (SI).

The procedure to simulate the cubic structure of the LMO has been the same as used to simulate an inverse spinel structure by the WIEN2k code when there exist, for example, the same ions in an octahedral site, but with different oxidation states. This is what happens, for example, in the inverse spinel structures of Fe_3O_4 ($Fe^{3+}_{tetrahedral}$)[$Fe^{2+}_{octahedral}$ $Fe^{3+}_{octahedral}$]O_4 and Co_3O_4 ($Co^{2+}_{tetrahedral}$)[$Co^{2+}_{octahedral}$ $Co^{3+}_{octahedral}$]O_4 which have structures restricted to the $Fd\bar{3}m$ space group with all 4 equivalent Fe ions or Co ions (octahedral). The primitive cell of LMO, in turn, is formed by ($Li^{1+}_{tetrahedral}$)[$Mn^{3+}_{octahedral}$ $Mn^{4+}_{octahedral}$]O_4, restricted to the $Fd\bar{3}m$ space group with the 4 equivalent Mn ions.

In order to differentiate the four Mn atoms, all 14 atoms were set to be crystallographically inequivalent. Then, the Mn atoms have been labeled differently, as Mn_1, Mn_2, Mn_3, and Mn_4. This forced the WIEN2k code calculations to consider them as inequivalent. The next step was to run the structure generator program that applies all possible symmetry operations to the given set of atoms in order to find a new space group for the crystal structure. As a result, a face-centered cubic structure has been recognized, with 9 inequivalent atoms: 1 Li, 4 Mn, and 4 O, and only 2 point group symmetries (inversion and identity). Finally, the atomic positions have been relaxed. As a result, the two pairs of the Mn ions in different oxidation states have been observed: Mn^{3+} at the positions (0.5, 0.5, 0.5) and (0.5, 0.75, 0.75), and Mn^{4+} at the positions (0.75, 0.5, 0.75) and (0.75, 0.75, 0.5), in terms of the lattice parameter a. As it will be shown in the next section, they differ in all analyzed

properties: structural, electronic, and magnetic. More details of the positions of all the atoms in the FCC cell generated by us can be observed in Table S1 of SI.

Knowing the spatial coordinates of each one of the Mn^{3+} and Mn^{4+} ions it was possible to perform simulations with different magnetic configurations. The magnetism in $LiMn_2O_4$ is the subject of much experimental controversy. There is a discussion about in which temperature a long-range magnetic order is observed (see Ref. [31] and references therein). For the cubic phase simulated by us at $T = 0$, we considered that the system is magnetically ordered. For that structure, we performed ferromagnetic (FM), antiferromagnetic (AFM), and FM and AFM combinations, as shown in Table S2 of SI. The magnetic ordering with the lowest energy was the same as found for the orthorhombic structure calculated by Liu et al. [29] with Mn^{3+} AFM (↑ ↓) and Mn^{4+} FM (↑ ↑).

3. Results and discussion

3.1. $LiMn_2O_4$ under ambient pressure

We started our study by calculating the structural, electronic, and magnetic properties of the LMO cubic structure under ambient conditions ($P = 0$). In the simulations, the atomic positions were relaxed according to equation S4 of SI. In turn, the optimization of the lattice parameters was realized using the Birch-Murnagham equations of states (equations S5 and S6 of SI) [32,33].

After the optimization process, the electronic structure and magnetic moments of Mn ions were calculated. Results are compared with experimental data in Table 1. These results show that the lattice parameters are in very good agreement with the experimental data, especially considering the functional GGA + U, with $U = 4.2$ eV. We did not find experimental data to compare the magnetic moments. Mn^{3+} has four unpaired d-electrons, Mn^{4+}, in turn, has three, so the magnetic moment of the Mn^{3+} ion should be larger than the magnetic moment of the Mn^{4+} ion. This configuration was indeed obtained by us in the cubic structure calculation. The Mn^{4+} - O bond lengths are 1.93 Å; in turn, the bond lengths of Mn^{3+} - O are 1.95, 1.96 Å in the xy plane and 2.13 Å along the z direction. This elongation along the z-direction is due to the JT distortion in the Mn^{3+} O_6 octahedron. The band gap of 0.5 eV is close to the experimental value of 0.37 eV. The value of the experimental specific capacity is smaller than the estimated theoretical value due to the fact that during the charge-discharge process not all Li ions are inserted or disinserted in the material. The experimental value is only 120 mAh/g, that is, the insertion and extraction of Li is only 0.8 per formula unit, that is, 80%. The calculated average voltage, in turn, is very close to the experimental value and in agreement with previous theoretical results [21,22,29].

Mn ions have the electronic configurations: Mn^{3+} (e^2_g, b^1_{2g}, a^1_{1g}, b^0_{1g}) and Mn^{4+} (t^3_{2g}, e^0_g). One can differentiate the two Mn atoms by inspection of the partial densities of states (PDOS) shown in Fig. 1. For Mn^{4+} ion, the t_{2g} energy levels (d_{xy}, d_{xz}, d_{yz}) with spin-up configuration are below the Fermi level, that is, the states are fully occupied. In turn, the t_{2g} energy levels with spin-down configuration, as well as the e_g energy levels ($d_{z^2}, d_{x^2-y^2}$) with spin-up and spin-down configurations, are above the Fermi level and are unoccupied states. The PDOS displayed in Fig. 1 is compatible with the $t^3_{2g}e^0_g$ electronic configuration of Mn^{4+} ion (d^3 configuration). For Mn^{3+} ion, the spin-up e_g (d_{xz}, d_{yz}), b_{2g} (d_{xy}), and a_{1g} (d_{z^2}) states are below the Fermi level and fully occupied, while the b_{1g} ($d_{x^2-y^2}$) level is unoccupied, consistent with the $e^2_g b^1_{2g} a^1_{1g} b^0_{1g}$ configuration of Mn^{3+} ion (d^4 configuration). The spin-down e_g, b_{2g}, a_{1g}, and b_{1g} orbitals are above the Fermi level and are all unoccupied states.

In this work, the face-centered cubic structure was able to describe the two oxidation states of the Mn ions of the LMO material, the JT distortion for the Mn^{3+} ion, the semiconducting state, and the ground state magnetic ordering. Therefore, we were able to verify the changes undergone in the LMO host matrix during lithium intercalation. These changes have already been theoretically investigated by considering either the orthorhombic [8,21,29,39] or cubic [22] phase of the LMO. Our results for the LMO properties with Li extraction agree with the previous theoretical [8,21,22,29,39] and experimental [38,39] results, which can be observed in Fig. S1 of SI.

3.2. $LiMn_2O_4$ under external pressure

For calculation of properties of the LMO under external hydrostatic pressure ($P > 0$), we utilized the same computational parameters as for the calculations at ambient pressure ($P = 0$), as well as the same functional GGA + U with $U = 4.2$ eV. Fig. 2 shows some of the properties calculated for the cubic LMO structure as a function of external pressure, ranging from 0 to 20 GPa. It can be observed that these properties change linearly with applied pressure.

Fig. 2 (a) shows the variation of the lattice parameter as a function of pressure. This result can be compared to that obtained experimentally by Lin et al. [3] who carried out a study of the LMO under high pressures using the X-ray diffraction technique. The lattice parameter values obtained theoretically are overestimated when compared to the experimental data over the whole range of the considered pressures. However, the same behavior of the lattice parameter, decreasing smoothly with the application of pressure, is observed in both the theoretical and experimental results. Fig. 2(b) describes the behavior of the unit cell volume as a function of pressure, and as expected, follows the same behavior pattern as the lattice parameter, that is, it decreases with pressure in a smooth and linear way. Fig. 2(c) shows the variation of the volume of the octahedrons ($Mn^{3+}O_6$ and $Mn^{4+}O_6$) when external pressure is applied. The volume of the octahedron around the Mn^{3+} ion exceeds the octahedron volume around the Mn^{4+} ion for all pressures considered. This is due to the fact that the octahedra containing Mn^{3+} ions exhibit larger bond lengths than octahedra containing Mn^{4+} ions, as shown in Fig. 2(d). The reason for this is the JT distortion around the Mn^{3+}, as discussed previously.

The electronic properties also exhibit smooth changes with increase of the pressure, keeping the arrangement and position of the Mn d-bands very similar to those shown in Fig. 1 for $P = 0$. In fact, the largest change perceived refers to the band gap value, which decreases smoothly with increasing pressure, as depicted in Fig. 3(a). The same behavior is observed for the magnetic moments of Mn^{3+} and Mn^{4+} ions at octahedral sites, i.e, they also decrease smoothly with increasing pressure, as displayed in Fig. 3(b).

After analyzing the structural, electronic, and magnetic properties of the cubic phase of the LMO under pressure, we investigated the possible transition from magnetic cubic (Cb-M) to magnetic orthorhombic (Ot-M) phase, experimentally suggested by Paolone et al. [18]. Furthermore, we simulated a possible non-magnetic cubic phase (Cb-NM) of this compound, since the external pressure can lead to a non-magnetic phase, as occurs, for example, with the Co_3O_4 spinel [40,41]. The Cb-NM phase is simulated using the same computational parameters as for the simulation of the Cb-M phase, but imposing zero magnetic moments for the Mn ions.

A summary of the structural, electronic, and magnetic properties

Table 1
Lattice parameter a (Å), valence states, magnetic moment (μ_B), band gap (eV), specific capacity (mAh/g), and average voltage (V) of the cubic phase of the LMO.

LMO	Theoretical	Experimental [3,34–38]
a = b = c	8.32	8.25
Mn valence state	Mn^{3+}/Mn^{4+}	Mn^{3+}/Mn^{4+}
Magnetic Moment	3.57/2.91	–
Specific capacity	148	120
Average voltage	3.95	4.1
Band gap	0.50	0.37

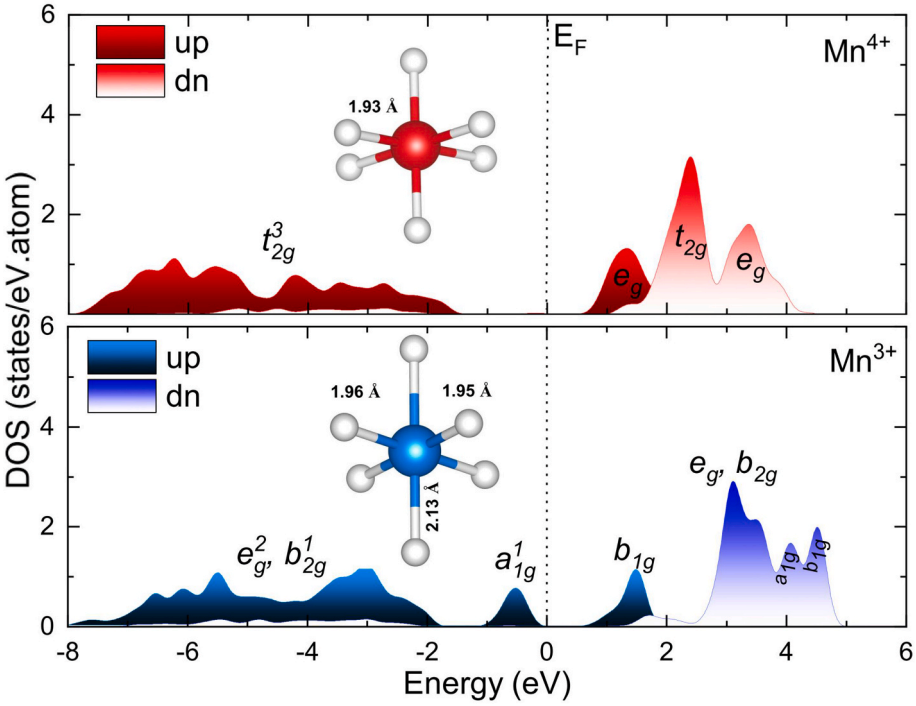

Fig. 1. Partial densities of states of LMO projected in the 3*d* orbitals of Mn^{3+} and Mn^{4+} ions, calculated using the GGA + U functional. The predominant orbitals are shown in each energy range considered. The dashed line denotes the Fermi level.

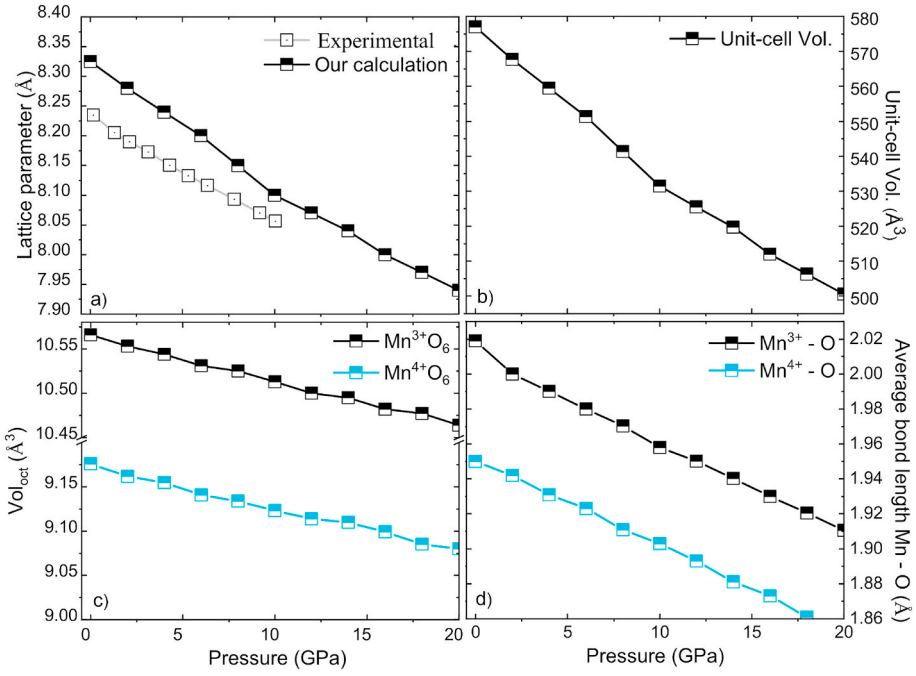

Fig. 2. (a) Lattice parameters, (b) unit cell volume, (c) octahedral volumes, and (d) Mn–O bond lengths at octahedral sites as a function of pressure for the cubic phase of the LMO. The lattice parameters (a) are compared to the experimental values obtained by Lin et al. [3].

obtained for all three calculated phases is shown in Table 2. Although the lattice parameters of these phases look different, the change in volume is in fact quite small. The values of the magnetic moments for Mn^{3+} and Mn^{4+} ions for the magnetic phases are very close. The band gaps calculated for the cubic and orthorhombic phases indicate that the Cb-M phase has a slightly higher electronic conductivity than the Ot-M one. The Cb-NM phase, in turn, has a vanishing band gap. The lattice parameters calculated for the orthorhombic structure agree with the experimental results [42] and with previous calculations [19].

After the successful simulation of the Cb-M, Cb-NM and Ot-M phases of the LMO, it was possible to calculate their enthalpy ($H = E + PV$) and to determine their relative stability in the considered pressure range. The result obtained for the enthalpy as a function of pressure can be seen in Fig. 4. From this result, one can analyze which LMO phase is more stable at each point of the considered pressure range. At $P = 0$ the orthorhombic structure exhibits lower energy than the magnetic cubic

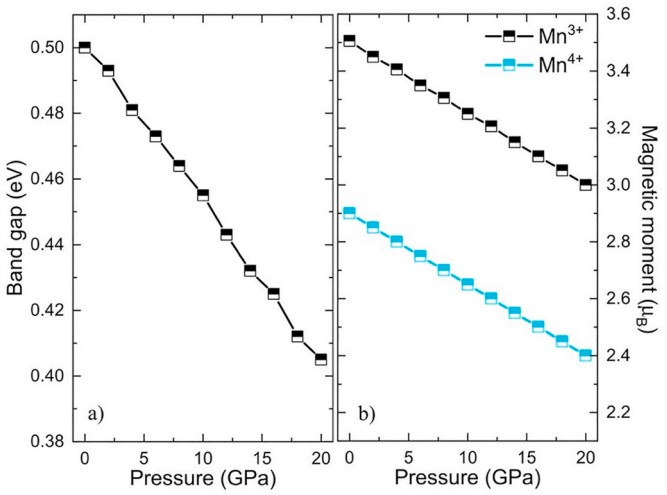

Fig. 3. Band gap (a) and magnetic moments of the Mn ions (b) of the cubic LMO as functions of pressure.

Table 2
Calculated equilibrium lattice parameters a,b,c (Å), valence states, magnetic moment (μ_B), and band gap (eV) of the CB-M, Cb-NM, and Ot-M phases of the LMO.

LMO	Cubic-M	Orthorhombic-M	Cubic-NM
a	8.32	8.24	8.13
b	8.32	8.19	8.13
c	8.32	8.34	8.13
Mn valence state	Mn^{3+}/Mn^{4+}	Mn^{3+}/Mn^{4+}	Mn
Magnetic moment	3.57/2.91	3.54/2.89	0.0
Band gap	0.50	0.55	0.0

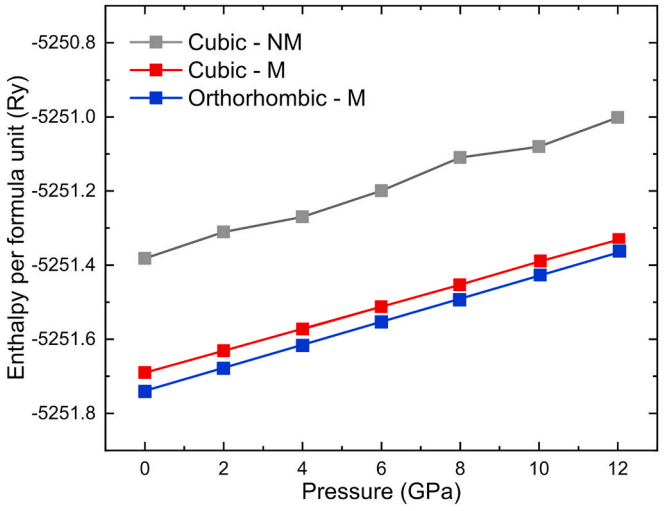

Fig. 4. Dependence of enthalpy per one formula unit ($LiMn_2O_4$) for Cubic-M, Cubic-NM, and Orthorhombic-M phases of the LMO.

structure, that is, the orthorhombic phase is the ground state structure. This result agrees with the conclusion of Liu et al. [29] who described the orthorhombic phase of LMO as the ground state phase at $P = 0$.

For $P > 0$, no transition from orthorhombic to cubic phase was observed for all pressures analyzed. The orthorhombic phase remains at lower energy even at high pressures. Therefore, the theoretical calculations do not confirm the existence of the Cb-M → Ot-M phase transition that had been predicted by Paolone et al. [18]. Our calculations agree with other experimental works that did not observe this transition (Cb-M → Ot-M) when analyzing LMO under hydrostatic and non-hydrostatic pressure [3,14–17]. Therefore, the Cb-M → Ot-M transition could occur only as function of temperature (below 280 K), but not of the hydrostatic pressure. The NM cubic phase, in turn, proved to be unfavorable in the entire pressure range considered, presenting an energy difference of 0.30 Ry (per formula unit) in relation to the cubic phase and of 0.36 Ry (per formula unit) to the orthorhombic phase at $P = 0$.

4. Conclusions

In this work, we used the density functional theory, in an GGA + U implementation, to calculate structural, electronic, and magnetic properties of the $LiMn_2O_4$ compound at ambient pressure, as well as to analyze the variation of these properties under elevated external hydrostatic pressures up to 20 GPa. We managed to describe the cubic phase of the material with different oxidation states of the Mn ions. At ambient pressure, Mn^{4+} - O bond lengths are found to be 1.93 Å, while Mn^{3+} - O bonds are 1.95–1.96 Å in the *xy* plane and 2.13 Å along the *z*-direction. Electronic properties determine different densities of states for Mn^{3+} (with one electron in the d_{z^2}-derived state) and Mn^{4+} (with an unoccupied d_{z^2}-derived state), with different magnetic moments of 3.57 μ_B for Mn^{3+} ion and 2.91 μ_B for Mn^{4+} ion.

The simulation of the $LiMn_2O_4$ under external pressure (up to 20 GPa) included the analysis of three different phases of the material: cubic magnetic, cubic-non-magnetic and orthorhombic one. The calculations under pressure demonstrated a standard behavior for the properties of the $LiMn_2O_4$, i.e, the lattice parameter, the unit cell volume, the octahedral volume around the Mn ions, the Mn–O bond lengths, the band gap width, and the magnetic moments of Mn^{3+} and Mn^{4+} ions decrease smoothly and linearly with increasing pressure. The enthalpy calculations revealed that the orthorhombic phase is the ground state structure and that the cubic → orthorhombic transition does not occur in all hydrostatic pressure range considered. A magnetic cubic to a non-magnetic cubic transition is proved to be quite unfavorable to form in the analyzed pressure range.

CRediT author statement

O. M. Sousa: Conceptualization, Investigation, Writing-Original Draft. **F. Sorgenfrei:** Validation, Writing-Original Draft. **L. V. C. Assali:** Methodology, Formal analysis,Writing- Review & Editing. **M. Lalic:** Formal anlysis, Writing- Review & Editing, Softwares, Resources. **A. B. Klautau:** Conceptualization, Writing-Review & Editing. **C. M. G Araujo**: Conceptualization, Methodology, Funding acquisition, Writing-Review & Editing. **P. Thunström:** Writing- Review & Editing. **O. Eriksson:** Conceptualization, Funding acquisition, Writing- Review & Editing. **H. M. Petrilli**: Supervision, Conceptualization, Methodology, Project administration, Funding acquisition, Writing- Review & Editing, Resources.

Declaration of competing interest

The authors declare that they have no known competing financial interests or personal relationships that could have appeared to influence the work reported in this paper.

Data availability

No data was used for the research described in the article.

Acknowledgements

HMP, LCVA, ABK and OMS acknowledge support from FAPESP (Project No 2020/00802-3); ML acknowledge FAPITEC; LVCA, HMP, ABK, ML and OMS acknowledge support from CNPq and CAPES, Brazil. The calculations were performed at the computational facilities of the

UFS/USP/CENAPAD-UNICAMP (Brazil). OE, PT, CMA and FS acknowledge support from the Knut och Alice Wallenberg (KAW) foundation, the Swedish Research Council (VR), the Foundation for Strategic Research (SSF), the Swedish energy agency (Energimyndigheten), eSSENCE, STandUP for energy, and the ERC (synergy grant FASTCORR).

Appendix A. Supplementary data

Supplementary data to this article can be found online at https://doi.org/10.1016/j.jpcs.2022.111198.

References

[1] D. Larcher, J.M. Tarascon, Towards greener and more sustainable batteries for electrical energy storage, Nat. Chem. 7 (2014) 19–29, https://doi.org/10.1038/nchem.2085.
[2] J.B. Goodenough, Energy storage materials: a perspective, Energy Storage Mater. 1 (2015) 158–161, https://doi.org/10.1016/j.ensm.2015.07.001.
[3] Y. Lin, Y. Yang, H. Ma, Y. Cui, W.L. Mao, Compressional behavior of bulk and nanorod $LiMn_2O_4$ under nonhydrostatic stress, J. Phys. Chem. C 115 (2011) 9844–9849, https://doi.org/10.1021/jp112289h.
[4] C.-G. Han, C. Zhu, G. Saito, T. Akiyama, Improved electrochemical properties of $LiMn_2O_4$ with the Bi and La co-doping for lithium-ion batteries, RSC Adv. 5 (2015) 73315–73322, https://doi.org/10.1039/C5RA13005K.
[5] Z. Cai, Y. Ma, X. Huang, X. Yan, Z. Yu, S. Zhang, G. Song, Y. Xu, C. Wen, W. Yang, High electrochemical stability Al-doped spinel $LiMn_2O_4$ cathode material for Li-ion batteries, J. Energy Storage 27 (2020), 101036, https://doi.org/10.1016/j.est.2019.101036.
[6] S. Bagcı, H.M. Tütüncü, S. Duman, E. Bulut, M. Özacar, G.P. Srivastava, Physical properties of the cubic spinel $LiMn_2O_4$, J. Phys. Chem. Solid. 75 (2014) 463–469, https://doi.org/10.1016/j.jpcs.2013.12.005.
[7] Y. Wu, C. Cao, J. Zhang, L. Wang, X. Ma, X. Xu, Hierarchical $LiMn_2O_4$ hollow cubes with exposed {111} planes as high-power cathodes for lithium-ion batteries, ACS Appl. Mater. Interfaces 8 (2016) 19567–19572, https://doi.org/10.1021/acsami.6b06820.
[8] J. Siqueira, C. Machado, D. Quattrociocchi, F. Garrido, L. da Costa, E. Ponzio, G. Ferreira, J. Resende, Experimental and theoretical study of $LiMn_2O_4$ synthesized by the solution combustion method using corn starch as fuel, J. Braz. Chem. Soc. 31 (2020) 381–393, https://doi.org/10.21577/0103-5053.20190192.
[9] J. Abou-Rjeily, I. Bezza, N.A. Laziz, C. Autret-Lambert, M.T. Sougrati, F. Ghamouss, High-rate cyclability and stability of $LiMn_2O_4$ cathode materials for lithium-ion batteries from low-cost natural $\beta-MnO_2$, Energy Storage Mater. 26 (2020) 423–432, https://doi.org/10.1016/j.ensm.2019.11.015.
[10] X. Li, J. Wang, S. Zhang, L. Sun, W. Zhang, F. Dang, H.J. Seifert, Y. Du, Intrinsic defects in $LiMn_2O_4$: first-principles calculations, ACS Omega 6 (2021) 21255–21264, https://doi.org/10.1021/acsomega.1c01162.
[11] P. Hohenberg, W. Kohn, Inhomogeneous electron gas, Phys. Rev. 136 (1964) B864–B871, https://doi.org/10.1103/PhysRev.136.B864.
[12] W. Kohn, L.J. Sham, Self-consistent equations including exchange and correlation effects, Phys. Rev. 140 (1965), https://doi.org/10.1103/PhysRev.140.A1133. A1133–A1138.
[13] Q. He, B. Yu, Z. Li, Y. Zhao, Density functional theory for battery materials, Energy Environ. Mater. 2 (2019) 264–279, https://doi.org/10.1002/eem2.12056.
[14] P. Piszora, W. Paszkowicz, W. Nowicki, R. Minikayev, C. Lathe, High-pressure phase transition in $LiMn_2O_4$, in: Jahresbericht/Hamburger Synchrotronstrahlungslabor HASYLAB Am Deutschen Elektronen-Synchrotron DESY= Annual Report, 2003, pp. 309–310.
[15] J. Darul, W. Nowicki, C. Lathe, P. Piszora, Observation of phase transformations in $LiMn_2O_4$ under high pressure and at high temperature by in situ X-ray diffraction measurements, Radiat. Phys. Chem. 80 (2011) 1014–1018, https://doi.org/10.1016/j.radphyschem.2011.02.011.
[16] P. Piszora, W. Nowicki, J. Darul, B. Bojanowski, S. Carlson, Y. Cerenius, Synchrotron X-ray diffraction studies of $LiMn_2O_4$ and $Li_4Mn_5O_{12}$ structures at high pressure, Radiat. Phys. Chem. 78 (2009) S89–S92, https://doi.org/10.1016/j.radphyschem.2009.03.086.
[17] P. Piszora, In-situ investigations of $LiMn_2O_4$ at high pressure, Z. Kristallogr. Suppl. 26 (2007) 387–392, https://doi.org/10.1524/9783486992540-061.
[18] A. Paolone, A. Sacchetti, P. Postorino, R. Cantelli, A. Congeduti, G. Rousse, C. Masquelier, Stabilization of an orthorhombic phase in LiMnO by means of high pressure, Solid State Ionics 176 (2005) 635–639, https://doi.org/10.1016/j.ssi.2004.10.007.
[19] C.Y. Ouyang, S.Q. Shi, M.S. Lei, Jahn–Teller distortion and electronic structure of $LiMn_2O_4$, J. Alloys Compd. 474 (2009) 370–374, https://doi.org/10.1016/j.jallcom.2008.06.123.
[20] A. Karim, S. Fosse, K.A. Persson, Surface structure and equilibrium particle shape of the $LiMn_2O_4$ spinel from first-principles calculations, Phys. Rev. B 87 (2013), 075322, https://doi.org/10.1103/PhysRevB.87.075322.
[21] W. Liu, H. Xu, Q. Zhou, Y. Dai, W. Hu, H. Li, The performance of Ni-doped spinel-type $LiMn_2O_4$ for Li-ion batteries: first-principles calculation, J. Electron. Mater. 49 (2020) 5523–5527, https://doi.org/10.1007/s11664-020-08298-1.
[22] B. Xu, S. Meng, Factors affecting Li mobility in spinel $LiMn_2O_4$—a first-principles study by GGA and GGA+U methods, J. Power Sources 195 (2010) 4971–4976, https://doi.org/10.1016/j.jpowsour.2010.02.060.
[23] D.J. Singh, L. Nordstron, Planewaves, Pseudopotentials and the LAPW Method, second ed., Springer, New York, 2006.
[24] P. Blaha, K. Schwarz, G.K.H. Madsen, D. Kvasnicka, J. Luitz, An Augmented Plane Waves + Local Orbital Program for Calculating Crystal Properties, Karlheinz Schwarz, Techn, Universitat Wien, Austria, 2001, pp. 1–223.
[25] J.P. Perdew, K. Burke, M. Ernzerhof, Generalized gradient approximation made simple, Phys. Rev. Lett. 77 (1996) 3865–3868, https://doi.org/10.1103/PhysRevLett.77.3865.
[26] V.I. Anisimov, J. Zaanen, O.K. Andersen, Band theory and Mott insulators: hubbard instead of stoner I, Phys. Rev. B 44 (1991) 943–954, https://doi.org/10.1103/physrevb.44.943.
[27] G.K.H. Madsen, P. Novák, Charge order in magnetite. An LDA + U study, Europhys. Lett. 69 (2005) 777–783, https://doi.org/10.1209/epl/i2004-10416-x.
[28] A.I. Liechtenstein, V.I. Anisimov, J. Zaanen, Density-functional theory and strong interactions: orbital ordering in Mott-Hubbard insulators, Phys. Rev. B 52 (1995) R5467–R5470, https://doi.org/10.1103/physrevb.52.r5467.
[29] W.-W. Liu, D. Wang, Z. Wang, J. Deng, W.-M. Lau, Y. Zhang, Influence of magnetic ordering and Jahn–Teller distortion on the lithiation process of $LiMn_2O_4$, Phys. Chem. Chem. Phys. 19 (2017) 6481–6486, https://doi.org/10.1039/C6CP08324B.
[30] L. Wang, T. Maxisch, G. Ceder, A first-principles approach to studying the thermal stability of oxide cathode materials, Chem. Mater. 19 (2006) 543–552, https://doi.org/10.1021/cm0620943.
[31] I. Tomeno, Y. Kasuya, Y. Tsunoda, Charge and spin ordering inLiMn2O4, Phys. Rev. B 64 (2001), https://doi.org/10.1103/physrevb.64.094422.
[32] F. Birch, Finite elastic strain of cubic crystals, Phys. Rev. 71 (1947) 809–824, https://doi.org/10.1103/PhysRev.71.809.
[33] F.D. Murnaghan, The compressibility of media under extreme pressures, Proc. Natl. Acad. Sci. USA 30 (1944) 244–247, https://doi.org/10.1073/pnas.30.9.244.
[34] M.J. Lee, S. Lee, P. Oh, Y. Kim, J. Cho, High performance $LiMn_2O_4$ cathode materials grown with epitaxial layered nanostructure for Li-ion batteries, Nano Lett. 14 (2014) 993–999, https://doi.org/10.1021/nl404430e.
[35] N. Nitta, F. Wu, J.T. Lee, G. Yushin, Li-ion battery materials: present and future, Mater. Today 18 (2015) 252–264, https://doi.org/10.1016/j.mattod.2014.10.040.
[36] Y.J. Wei, X.G. Xu, C.Z. Wang, C. Li, G. Chen, F. Wu, Electronic structure of cubic Li$(Fe_{0.1}Mn_{1.9})O_4$ studied with Mössbauer spectroscopy and first-principles calculation, Appl. Phys. Lett. 83 (2003) 1791–1793, https://doi.org/10.1063/1.1606494.
[37] K. Kushida, K. Kuriyama, Observation of the crystal-field splitting related to the Mn-3d bands in spinel-$LiMn_2O_4$ films by optical absorption, Appl. Phys. Lett. 77 (2000) 4154–4156, https://doi.org/10.1063/1.1336552.
[38] W. Liu, K. Kowal, G.C. Farrington, Mechanism of the electrochemical insertion of lithium into $LiMn_2O_4$ spinels, J. Electrochem. Soc. 145 (1998) 459–465, https://doi.org/10.1149/1.1838285.
[39] T. Okumura, Y. Yamaguchi, M. Shikano, H. Kobayashi, Further findings of X-ray absorption near-edge structure in lithium manganese spinel oxide using first-principles calculations, J. Mater. Chem. A. 2 (2014) 8017–8025, https://doi.org/10.1039/C3TA15412B.
[40] O.M. Sousa, J.S. Lima, A.F. Lima, M.V. Lalic, Theoretical study of structural, electronic and magnetic properties of the spinel Co_3O_4 under the pressure from 0 to 30 GPa, J. Magn. Magn Mater. 484 (2019) 21–30, https://doi.org/10.1016/j.jmmm.2019.03.122.
[41] F. Cova, M.V. Blanco, M. Hanfland, G. Garbarino, Study of the high pressure phase evolution of Co_3O_4, Phys. Rev. B 100 (2019), 054111, https://doi.org/10.1103/PhysRevB.100.054111.
[42] K. Sato, D.M. Poojary, A. Clearfield, M. Kohno, Y. Inoue, The surface structure of the proton-exchanged lithium manganese oxide spinels and their lithium-ion sieve properties, J. Solid State Chem. 131 (1997) 84–93, https://doi.org/10.1006/jssc.1997.7348.